ADVANCED ENGINEERING MATERIALS

DOI: 10.1002/adem.201300524

Geometry-Induced Mechanical Properties of Carbon Nanotube Foams**

By *Ludovica Lattanzi, Luigi De Nardo, Jordan R. Raney* and *Chiara Daraio**

Carbon nanotube (CNT) foams have unmatched energy absorption properties derived from their complex hierarchical structure. The control of the micro-scale geometry of these foams allows tuning their behavior to specific application-driven needs. Geometrical structures in CNT foams are obtained by synthesizing CNTs on substrates patterned with different growth templates: circles, lines and concentric rings. To study the effects of the microstructural geometry on the bulk mechanical response of the foams, the samples are tested under cyclic quasi-static compressive deformation (up to 50% strain). The geometry of the patterns plays a fundamental role on the samples' macroscopic energy absorption capability, maximum stress, and strain recovery. Patterned CNT structures demonstrated mechanical properties comparable or improved over non-patterned, bulk CNT foams, but with much lower density. Quasi-static compressive tests performed on different patterned structures with the same effective density ($\rho = 0.02\,g\,cm^{-3}$) exhibit considerably different responses. For example, the stress reached by foams patterned in concentric rings is ≈15 times higher than that observed for pillars and lines. The results show how the mechanical response of CNT foams can be tailored by varying the CNT microstructural architecture.

1. Introduction

The hierarchical organization of the structure of natural materials is the basis of bio-inspired design.[1] Synthetic materials with hierarchical structures at different scales can be realized with properties tailored to specific applications.[1,2] However, to realize synthetic materials with tailored properties, it is essential to understand the structure/function relationships governing the material responses, and to develop suitable manufacturing technologies. Metamaterials,[3] bio-inspired materials,[4,5] lab-on-chip systems[6–8] and scaffolds for tissue engineering applications[9] are some examples in which well-defined structures with novel geometries are required in order to obtain improved performance.

Due to their high aspect ratio and exceptional mechanical properties, carbon nanotubes (CNTs) have been used in nanostructured composites,[10] and have been assembled to create stand-alone multi-scale macroscopic structures.[11] Understanding the effects of length scale and geometry of the microstructure of materials is particularly important to control and improve their mechanical response.[12] Stand-alone CNT arrays were combined with polymers to create macro-scale hybrid structures,[13] in which the alignment and the hierarchy improve the inter-laminar strength and toughness,[14] flexural modulus, electrical conductivity[15] and energy absorption capability.[16]

Several recent studies have examined the properties of CNT microstructures, synthesized on micro-patterned growth substrates, for different applications. Copic *et al.*[17] demonstrated that vertically aligned CNT (VACNT) patterns, including vertical micro-pillars and honeycomb lattices with sub-micron wall thickness, could be used as master molds for

[*] *Prof. C. Daraio, L. Lattanzi, Dr. J. R. Raney*
Engineering and Applied Science, California Institute of Technology, 91125 Pasadena, CA, USA
E-mail: daraio@ethz.ch
Prof. L. De Nardo, L. Lattanzi
Department of Chemistry, Materials and Chemical Engineering "G. Natta", Politecnico di Milano 20131 Milan, Italy
Dr. J. R. Raney
Department of Mechanical Engineering, Baylor University, 76798 Waco, TX, USA
Prof. C. Daraio
Department of Mechanical and Process Engineering, Swiss Federal Institute of Technology (ETH), 8092 Zürich, Switzerland

[**] *This work is supported by the Institute for Collaborative Biotechnologies, under contract W911NF-09-D-0001 with the Army Research Office. We thank the Kavli Nanoscience Institute at Caltech for the use of nanofabrication facilities.*

precise fabrication of polymer micro-devices. A wide variety of 3D corrugated VACNT microstructures were realized, reproducing the geometry of macro-scale folded structures, and showed potential for use as out-of-plane microsprings with compliance dependent on the wall thickness and number of folds.[18] Li *et al.*[19] realized micro-scale flexible systems using interconnected VACNT lines impregnated in a PDMS matrix with gold electrodes, for use as flexible sensors, actuators and microfluidic devices.

The macroscopic mechanical response of 3D VACNT forests (i.e. unpatterned VACNTs) and the advantages that arise due to their fibrous and multiscale structure were previously described.[16,20,21] The properties of these systems (e.g. energy absorption capability, recoverability, buckling mode, and viscoelasticity) depend on the fabrication method, on the internal structure, and on the density. For instance Xu *et al.*[22] demonstrated how the viscoelastic properties of CNT materials could be tailored by tuning the density through controlling the reactive ion etching exposure time. Shaping the microstructure is used to make structures lighter maintaining the same stiffness.[23] The synthesis process plays a fundamental role in determining the structure and the properties of VACNT ensembles, including the morphology, compliance, energy absorption, recoverability and density.[24–30]

Despite this progress, the effects of the structural hierarchy at the nanometer and micrometer scale on the resultant bulk properties are still elusive. Here, we describe the fabrication and the mechanical properties of micro-patterned VACNT structures. The VACNTs are grown on Si substrates patterned with three different geometries, as shown in Figure 1. The effect of the structural architecture on the bulk mechanical response is studied by performing cyclic quasi-static compressive tests.

2. Results and Discussion

We studied three different pattern geometries: pillars, lines and concentric ring columns, as shown in Figure 1. The pillars and the lines have a fixed diameter and thickness, respectively, and are spaced by using different gap values. The columns are composed of three concentric rings and are patterned in a squared array, in contact.

All VA CNTs are ≈1.8 mm tall and are grown on silicon rectangles with a cross sectional area of about 20.5 ± 0.5 mm^2. The density of the patterned structures, defined as the effective density, is calculated by dividing the weight of the VA CNTs by their volume.

Misra *et al.*[31] observed that the position of a VACNT sample on its silicon growth substrate affected the density of the CNT forests. Samples closer to the entrance of the feed solution exhibited higher density. Our results show the same behavior, for both non-patterned and patterned substrates, explaining the range of effective density measured for each structure (Figure 2). The density gradient resulting from the chemical vapor deposition (CVD) process also explains why structures characterized by different filling fraction, e.g. CNT forests and 100 μm thick VACNT lines with 2 μm sized gaps, can have the same effective density.

Figure 2 shows the energy absorption capability of the different structures. It is evident that the energy absorption depends on the effective density of the sample, as well as on the geometry of their microstructure. For example, structures composed by lines 100 μm thick and gap 100 μm exhibit lower energy absorption than the substrate made up of lines 100 μm thick and gap 2 μm, at the same density ($\rho = \approx 0.05$–0.07 g cm^{-3}).

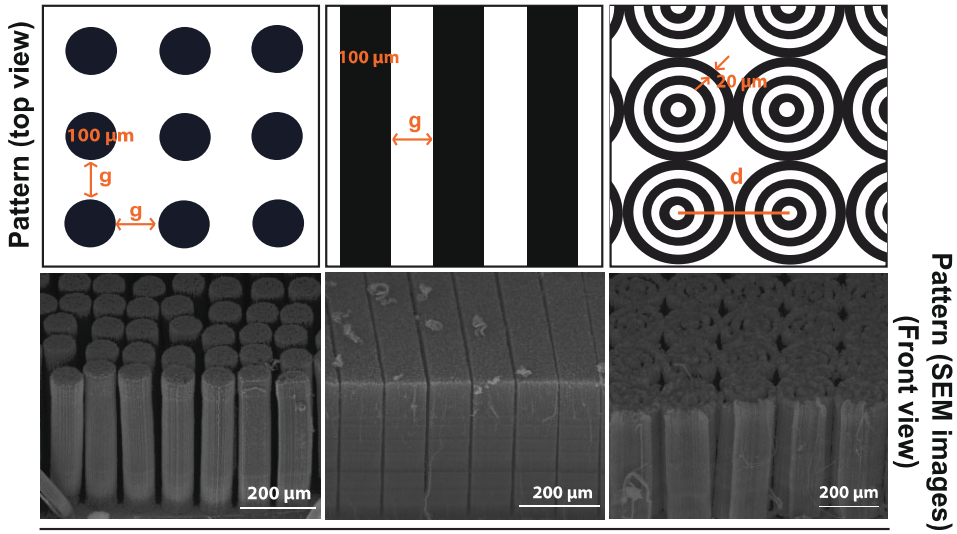

Fig. 1. SEM images of the CNT patterned structures and the respective dimensions and structural architecture (gaps).

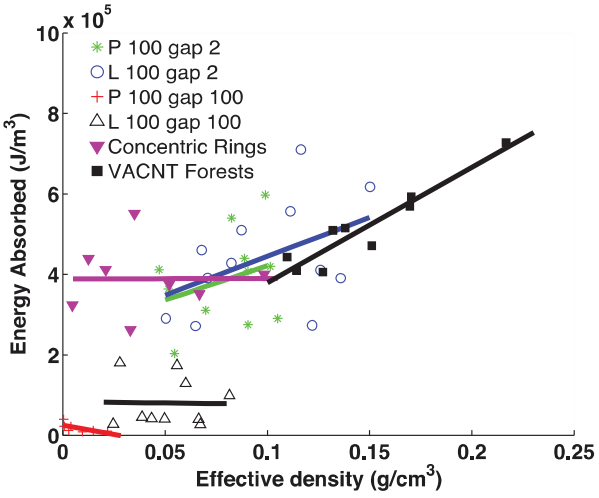

Fig. 2. Energy absorbed as a function of the effective density for the different CNT patterned structures (where P 100 = Pillars with diameter 100 μm and L 100 = Lines with thickness 100 μm).

Figure 2 also shows that structures with different filling fractions and densities have comparable energy absorption capability. The results clearly demonstrate the fundamental role of the structural organization. Despite the low density ($\rho = \approx 0.01$–$0.1\,g\,cm^{-3}$) of the patterns made by concentric rings, their energy absorption capability is comparable to that observed in VACNT forests ($\rho = \approx 0.1$–$0.25\,g\,cm^{-3}$), showing the large effect of geometry in the bulk mechanical response.

Stress–strain curves as a function of gap size (g) for line and pillar patterns (Figure 3a and b, respectively) were also analyzed. Results show that increases in the gap correlate with an overall reduction of the bulk peak stress. There is a critical gap value under which the stress reached by the patterned structures (pillars and lines) is comparable to that observed in non-patterned structures (VACNT forests). Above this critical gap size, the stress drops, as shown in Figure 3a and b. The higher stress values for the small gap cases (e.g. 2 μm for lines and 0 and 2 μm for pillars) result from the fact that the buckling structures are close enough to one another that they come into contact during deformation. As a result, the individual CNTs can interact dissipatively with one another due to the rapid formation and breaking of van der Waals interactions.[32] Bedewy *et al.*[33] reported the behavior of CNT–CNT interactions as a function of the distance between CNTs inside the forest, modeling the CNTs as hollow cylinders lying in the same plane. Mechanical reinforcement was shown when two CNTs are compressed and buckle towards each other.[33] A similar mechanical reinforcement occurs when the lines and the pillars with small gaps (e.g. 0 and 2 μm) start buckling and are drawn together. This lateral interaction between structures does not occur at higher gap sizes, explaining why, in this case, the stress decreases.

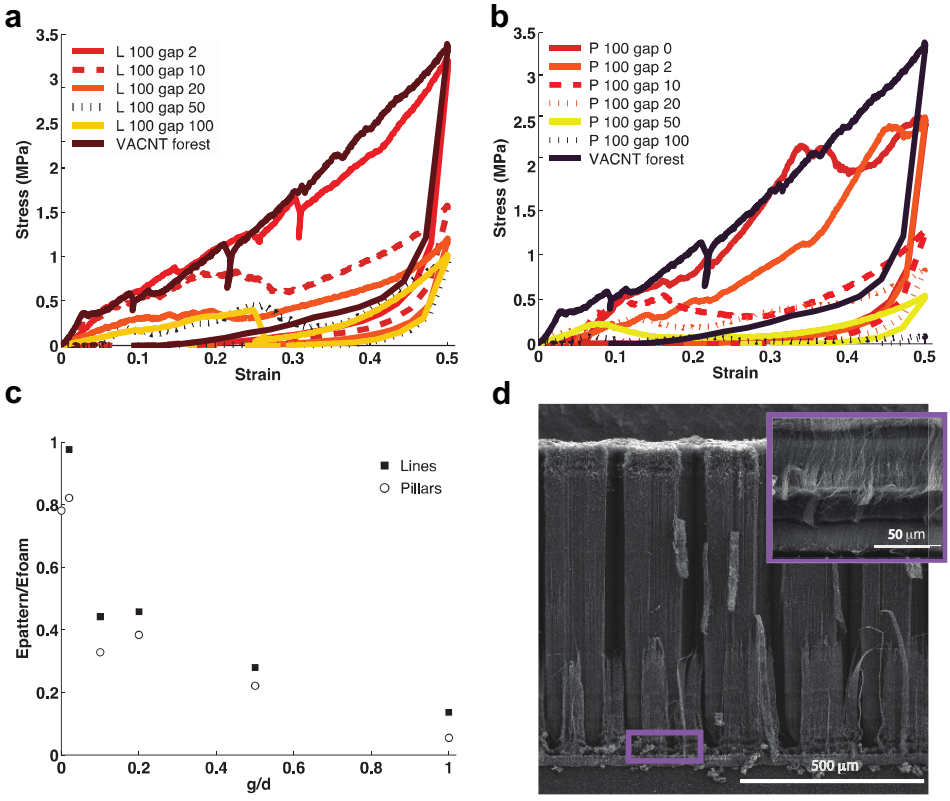

Fig. 3. Effect of the microstructural architecture on the mechanical properties. (a) and (b) Stress–strain curves as a function of gap for line and pillar patterns, respectively. (c) Ratio of the energy absorption of patterned and non-patterned structures as a function of g/d (where g is the gap and d the thickness of the lines or the diameter of the pillars). (d) SEM image of concentric rings after compression (front view). The inset shows the amplification of the buckling region.

We analyzed the buckling of the patterned structures using scanning electron microscope (SEM; Figure 3d). The presence of undulations in the stress–strain curves (Figure 3a and b) correlates with the formation of buckles in compression. Similar undulations were also reported earlier in the compression of single CNT pillars[34,35] and in the indentation of VACNT micro-muffins.[36] It is interesting to notice that the mechanical response observed in single pillars (e.g. the wave-like shape and the nonzero positive slope of the plateau region, due to the vertical property gradient in the VACNT pillar[36]) is also observed in a macroscopic multiscale structure made of multiple pillars.

The mechanical performance of different geometrical patterns at the same gap sizes is also reported in Figure 3. The stress reached by the line pattern is slightly higher then the stress observed in the pillar structures because of the different moment of inertia and filling fraction (A_{CNT}/A_{Sample}, where A_{CNT} is the area occupied by the CNTs and A_{Sample} is area of the sample) that on equal substrate area is 0.97 and 0.68 for lines and pillars pattern, respectively. The CNT pattern geometry plays an important role in particular at high gap values (e.g. 100 μm). At such gaps, the stress reached by lines is ≈20 times higher than the stress shown by pillars. This could be partially explained by the different filling fractions of the lines and pillars for gaps of 100 μm, which are 0.5 and 0.19, respectively. Under compression the lines buckle and eventually collapse, causing the stress–strain behavior to shift into the densification regime. Such high densification regime is not observed in the pillar structures.

Figure 3c shows the ratio of the energy absorption of both, patterned and non-patterned structures (VACNT forests) as a function of the microstructure architecture g/d (where g is the gap size and d the thickness of the lines or the diameter of the pillars).

The results show that at 2 μm gap the lines have the same energy absorption capability of the VACNT forests, while the pillars exhibit a slightly lower energy absorption. Above the critical gap value, the energy absorption capability is drastically reduced to about half the energy absorption of bulk VACNT forests. One explanation for this effect can be found in the work of Xu *et al.*, where it was shown that the energy dissipation in random networks of CNTs is due to zipping and unzipping of nodes. It was observed that with decreasing number of detachable nodes the energy dissipation decreased.[37]

We carried out quasi-static compressive tests on concentric rings, lines, and pillars with the same effective density ($\rho = 0.02\,g\,cm^{-3}$). The results (Figure 4) show a considerable difference of the stress–strain curves for the different geometries. The stress reached by concentric rings is ≈15 times higher than that observed for pillars and lines. Interestingly, the maximum stress measured for concentric rings has the same value of the stress reached by bulk VACNT forests, although the bulk forests have about 30% higher bulk density. These results suggest that the geometry of the microstructure plays a fundamental role in the mechanical performance and can be used in materials design.

The microstructural geometry affects also the recovery of deformation. After compression to 0.5 strain, concentric ring patterns recover up to ≈85% of the initial length, while lines and pillars recover ≈44% and ≈14%, respectively.

Previous studies stated that the recoverability of CNT ensembles, such as sponges, is highly dependent on bulk density.[38] Here, we show that, at the same bulk density, the recovery can be controlled by the structural architecture.

Stiffness changes in the post-elastic regime as a function of geometry and maximum strain are shown in Figure 5. The trends observed in stiffness variations confirm the previous observations. At the same bulk density, concentric ring structures are stiffer than pillar and line patterns (with gap of 100 μm). The different deformation mechanisms are presented in Figure 5. It is evident from the presence of undulations in the stress–strain curves that buckling occurs earlier in concentric ring patterns than in bulk VACNT forests. Between 0.3 and 0.4 strain the elastic modulus drops to ≈80 MPa for concentric rings and increases to ≈115 MPa for CNT forests. Due to the larger gap (100 μm) the line and the pillar patterns show a lower elastic modulus, correlated to earlier buckling and structural collapse of the structures. As seen in Figure 3a, at ≈0.25 strain, lines with 100 μm gap exhibit

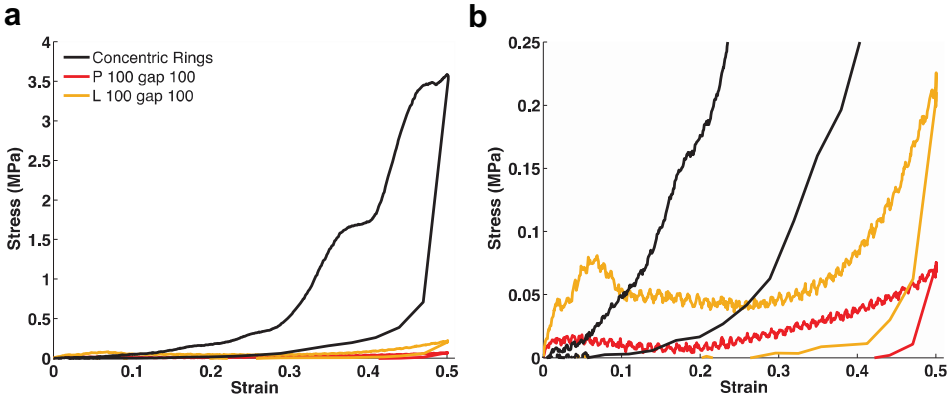

Fig. 4. (a) Plot of the stress–strain curves of same density structures as a function of the geometry. (b) Amplification of the first region of the curves up to $\sigma_{max} = 0.25$ MPa.

ADVANCED ENGINEERING MATERIALS

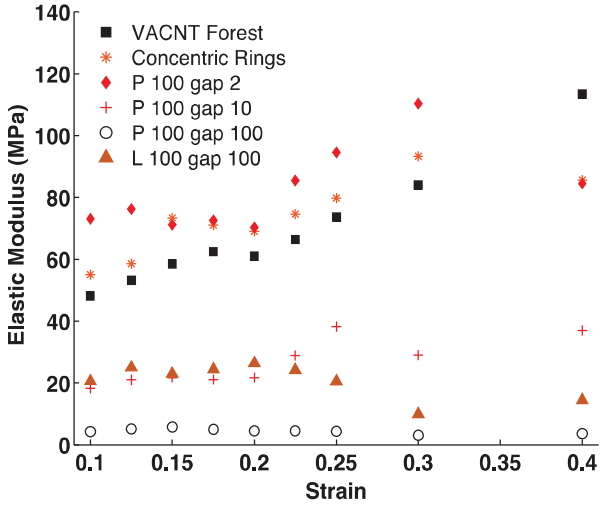

Fig. 5. Variation of the elastic modulus as a function of the strain for CNT patterned structures.

a large buckle, causing a decrease in the measured stress and elastic modulus.

3. Conclusion

In this study, we characterized the effects of pattern geometry on the mechanical response of VACNT foams. We showed that the structural architecture plays a fundamental role in determining energy absorption, peak stress and recovery from deformation. We fabricated lighter structures preserving the mechanical response of bulk CNT foams. For example, we showed that CNTs organized in concentric rings reach peak stress comparable to bulk CNT forests, although with lower density. This approach could allow the fabrication of new CNT-based devices and composite materials characterized by novel properties, excellent mechanical response and ultra low weight.

4. Experimental

4.1. VACNT Synthesis

The micro-patterned VACNTs were grown on silicon wafers by CVD. At the temperature of 827 °C, a solution of ferrocene in toluene ($[w/v] = 20\,g\,L^{-1}$) was injected into a quartz tube inside an argon flow of 800 SCCM (cubic centimeters per minute at standard temperature and pressure).[20]

4.2. Photolithography of Silicon Wafer

The Silicon wafers were dehydrated at 130 °C for 60 s on a hot plate and Hexamethyldisilazane (HDMS) primer was deposited by evaporation for 300 s. AZ positive photoresist was spin coated on the substrates and then baked at 110 °C for 120 s. The samples were exposed under a mask with desired geometry for 3 s at 330 W. After the developer bath, a chromium thin film was evaporated onto the silicon wafer.

The undeveloped photoresist was removed in an acetone bath. The remaining chromium thin film acted as a negative mask, preventing CNT growth in selected areas of the wafer.

4.3. Mechanical Characterization

The VACNT structures were tested in compression, on their growth substrate, using an Instron 3000 electropulse dynamic test system at room temperature. A pre-load of 0.5 N was applied to all samples in order to provide uniform contact between the sample's surfaces and the compression platens. Quasi-static four-cyclic tests were performed using strain value of 0.5 applied at a strain rate of $0.03\,s^{-1}$. The energy absorbed per unit volume by the CNT samples under compressive load was calculated by integrating the area within the hysteresis loop in the stress–strain curve. The elastic modulus at the different strain values was calculated by performing a series of unloading steps at strains ranging from 0.1 to 0.4 during a compression test and measuring the slope of the unloading in the stress–strain curve.

Received: November 11, 2013
Final Version: December 12, 2013

[1] F. Xia, L. Jiang, *Adv. Mater.* **2008**, *20*, 2842.
[2] B. Bhushan, Y. C. Jung, *Prog. Mater. Sci.* **2011**, *56*, 1.
[3] J. K. Gansel, *Science* **2009**, *325*, 1513.
[4] H. Lee, B. Bhushan, *J. Colloid Interf. Sci.* **2012**, *372*, 231.
[5] B. Bhushan, *Beilstein J. Nanotechnol.* **2011**, *2*, 66.
[6] F. Evenou, J. Di Meglio, B. Ladoux, P. Hersen, *Lab Chip* **2012**, *12*, 1717.
[7] C. H. Chuang, Y. H. Huang, Y. T. Wu, *Biomed. Microdev.* **2012**, *14*, 271.
[8] S. S. Kallempudi, Z. Altintas, J. H. Niazi, Y. Gurbuz, *Sens. Actuat. B* **2012**, *163*, 194.
[9] A. Béduer, C. Vieu, F. Arnauduc, J. C. Sol, I. Loubinoux, L. Vaysse, *Biomaterials* **2012**, *33*, 504.
[10] R. F. Gibson, *Compos. Struct.* **2010**, *92*, 2793.
[11] L. Liu, Z. Ma, Wand. Zhang, *Small* **2011**, *11*, 1504.
[12] L. J. Bonderer, A. R. Studart, L. J. Gauckler, *Science* **2008**, *319*, 1069.
[13] A. Misra, J. R. Greer, C. Daraio, *Adv. Mater.* **2009**, *21*, 334.
[14] E. J. Garcia, B. L. Wardle, A. J. Hart, *Compos. Part A* **2008**, *39*, 1065.
[15] V. P. Veedu, A. Cao, X. Li, K. Ma, C. Soldano, S. Kar, P. M. Ajayan, M. N. Ghasemi-Nejhad, *Nat. Mater.* **2006**, *5*, 457.
[16] A. Misra, J. R. Raney, L. De Nardo, A. E. Craig, C. Daraio, *ACS Nano* **2011**, *5*, 7713.
[17] D. Copic, S. J. Park, S. Tawfick, M. F. L. De Volder, A. J. Hart, *Lab Chip* **2011**, *11*, 1831.
[18] M. F. L. De Volder, S. Tawfick, S. J. Park, A. J. Hart, *ACS Nano* **2011**, *5*, 7310.
[19] B. Li, M. G. Hahm, J. L. Kim, H. Y. Jung, S. Kar, Y. J. Jung, *ACS Nano* **2011**, *5*, 4826.
[20] L. Lattanzi, J. R. Raney, L. De Nardo, A. Misra, C. Daraio, *J. Appl. Phys.* **2012**, *111*, 1.
[21] A. Cao, P. L. Dickrell, W. G. Sawyer, M. N. Ghasemi-Nejhad, P. M. Ajayan, *Science* **2005**, *310*, 1307.
[22] M. Xu, D. N. T. Futaba, M. Yumura, K. Hata, *Nano Lett.* **2011**, *11*, 3279.

[23] L. J. Gibson, M. F. Ashby, B. A. Harley, *Cellular Materials in Nature and Medicine*, Cambridge University Press, New York, USA **2010**.
[24] S. B. Hutchens, L. J. Hall, J. R. Greer, *Adv. Funct. Mater.* **2010**, *20*, 2338.
[25] J. R. Raney, A. Misra, C. Daraio, *Carbon* **2011**, *49*, 3631.
[26] J. R. Raney, R. Y. Wang, C. Daraio, *Carbon* **2013**, *52*, 193.
[27] C. P. Deck, J. Flowers, G. S. B. McKee, K. Vecchio, *J. Appl. Phys.* **2007**, *101*, 023512.
[28] O. Yaglioglu, A. Cao, A. J. Hart, R. Martens, A. H. Slocum, *Adv. Funct. Mater.* **2012**, *22*, 5028.
[29] P. D. Bradford, X. Wang, H. Zhao, Y. T. Zhu, *Carbon* **2011**, *49*, 2834.
[30] C. M. McCarter, R. F. Richards, S. Dj. Mesarovic, C. D. Richards, D. F. Bahr, D. McClain, J. Jiao, *J. Mater. Sci.* **2006**, *41*, 7872.
[31] A. Misra, J. R. Raney, A. E. Craig, C. Daraio, *Nanotechnology* **2011**, *22*, 1.
[32] Y. Xiaodong, H. Pengfei, G. Huajian, *Nano Res.* **2011**, *4*(12), 1191.
[33] M. Bedewy, E. R. Meshot, H. Guo, E. A. Verploegen, W. Lu, A. J. Hart, *J. Phys. Chem. C* **2009**, *113*, 20576.
[34] Y. Onnik, *Ph. D. Thesis*, Massachusetts Institute of Technology, USA **2007**.
[35] B. Shelby, L. Hutchens, J. Hall, J. R. Greer, *Adv. Funct. Mater.* **2010**, *20*, 2338.
[36] S. Pathak, E. J. Lim, P. P. S. S. Abadi, S. Graham, B. A. Cola, J. R. Greer, *ACS Nano* **2012**, *6*, 2189.
[37] M. Xu, D. N. Futaba, T. Yamada, M. Yumura, K. Hata, *Science* **2010**, *330*, 1364.
[38] X. Gui, J. Wei, K. Wang, A. Cao, H. Zhu, Y. Jia, Q. Shu, D. Wu, *Adv. Mater.* **2010**, *22*, 617.

